TURBIDITY MAPPING AND PREDICTION IN ICE MARGINAL LAKES AT THE
BERING GLACIER SYSTEM, ALASKA

by

Liza K. Liversedge

A thesis submitted
in partial fulfillment of the requirements
for the degree of
Master of Science
(Natural Resources and Environment)
in the University of Michigan
December 2007

Thesis Committee:

      Professor Michael J. Wiley, Chair
      School of Natural Resources and Environment

      Professor Guy A. Meadows
      College of Engineering

      Adjunct Associate Professor Robert A. Shuchman
      College of Engineering

Acknowledgements

Table of Contents

List of Figures

List of Tables

Abstract

Turbidity mapping and prediction using remote sensing has had limited success in the past. Previous research efforts have been conducted in temperate and even tropical climates where too many confounding factors affect the remote sensing signal. My research is focused on the development of an accurate and repeatable algorithm to predict turbidity in northern, glacial lakes using electro-optical satellite data.

From an evolutionary perspective glacial environments are highly immature. Lakes found in these environments are typically classified as extremely oligotrophic resulting from their relatively recent formation and the surrounding harsh, northern climate. Unlike temperate or tropical lakes, northern glacial lakes do not contain significant amounts of biological material. Instead, these lakes are dominated by rock flour – suspended sediment originating from glacial rock weathering. This lack of biological influence makes satellite turbidity mapping and prediction more straightforward and potentially more accurate than similar efforts in temperate or tropical environments where biology typically drives these systems and strongly affects the remotely-sensed, electro-optical signal.

The study site for my research was an ice marginal lake at the Bering Glacier located in coastal, south central Alaska. In situ turbidity data, collected using an autonomous robot buoy, was used to develop a model-based turbidity algorithm. Simple and multiple linear regression analyses were conducted using different Landsat 7 ETM+ bands to determine the best predictor(s) of turbidity in glacial lakes. The final algorithm utilized Landsat 7 ETM+ Band 3 (red portion of the electromagnetic spectrum) and Band

4 (near-infrared portion of the electromagnetic spectrum) data to predict turbidity concentrations.

Turbidity maps created using the algorithm can be used to help determine inter- and intra-annual sediment dynamics of Vitus Lake. This information could be used to help researchers predict significant glacial events such as outburst floods or surge events. The turbidity maps could also provide insight into the hydrologic routing of the Bering Glacier system by showing where the Glacier is discharging sediment-laden freshwater into Vitus Lake through subsurface conduits. The turbidity algorithm also has broader applicability to other glacial lakes in south central Alaska and potentially glacial lakes worldwide.

Key words: glaciers, remote sensing, Landsat, GIS, turbidity, ALWAS, ice marginal lakes, Bering Glacier, Alaska

Introduction

Detecting and assessing water quality parameters from space is an emerging field. Scientists have been observing water bodies from space for as long as satellite remote sensing has been available, but specific techniques and algorithms for accurate and repeatable measurements of water parameters are only beginning to appear in the literature.

Previous research has been focused on extracting water quality parameters such as chlorophyll-a, total phosphorous, suspended solids, secchi disk depth, turbidity, salinity, temperature, and colored dissolved organic material, among others. Accuracy of these research efforts has varied depending on the parameter of interest, type of aquatic system under investigation, remote sensing platform used, and geographical area of study. Unfortunately, very few of these efforts have resulted in the development of products or methods useful beyond a specific image scene or small area of study.

Much of the work on remote sensing of water quality has occurred in the American Midwest, specifically Wisconsin, Minnesota, and to a lesser extent Michigan. These states have been working to develop a trophic state index for their inland lakes using volunteer secchi disk data and Landsat satellite data (Upper Midwest Regional Earth Science Applications Center). The Laurentian Great Lakes in particular have been popular for aquatic remote sensing applications such as assessing and quantifying color producing agents (CPAs) of these water bodies using SeaWiFS (Sea-viewing Wide Field-of-view Sensor) and MODIS (Moderate Resolution Imaging Spectroradiometer) satellite data (Pozdnyakov, Shuchman et al. 2005) (Shuchman, Korosov et al. 2006). Most of the

3

aquatic remote sensing research has been conducted in temperate climates, while very little research has occurred in northern environments.

My research is focused on remote sensing of turbidity in northern, glacial lakes. These lakes receive large inputs of sediment from glacial processes, and this sediment is clearly visible from space and easily measured in situ. The suspended sediment is principally rock flour – rock crushed to a powder by a moving glacier – and this is virtually the only substance contributing to the high values of turbidity found in these environments. Since there are little other materials, biological or physical, confounding the remotely-sensed optical signal, delineation of turbidity concentrations in glacial environments is more straightforward and accurate than similar efforts in temperate or tropical climates where biology typically drives aquatic systems and strongly affects the optical signal.

In general, aquatic systems are comprised of living, non-living, and once-living materials. These components, along with air bubbles and inhomogeneities resulting from small-scale water eddies, determine the optical properties of natural water bodies (Pozdnyakov and Grassl 2003). The major CPAs for non-Case I waters are phytoplankton, bacterioplankton, dissolved organic carbon, suspended mineral matter, detritus, and potentially air bubbles (Pozdnyakov and Grassl 2003). Of the CPAs, glacial lakes typically only contain significant amounts of suspended mineral matter (rock flour). These lakes lack the other CPAs since they are highly oligotrophic – a result of their relative immaturity from an evolutionary perspective and their harsh climates.

There is little agreement among researchers on the strength, form, or even optimum wavelengths to be used in determining the relationship between in situ turbidity

measurements and satellite radiance/reflectance data (Novo, Hansom et al. 1989). For example, Baban (1993) combined a variety of different mathematical operators (addition, subtraction, multiplication, division, exponents) and Landsat bands, but found that the best predictor of various water quality parameters in the Norfolk Broads, United Kingdom were one-band predictors. Specifically, Baban (1993) found that Landsat 5 TM Band 1 (Table 1) was the best predictor for secchi disk depth and suspended solids. Brezonik, Menken et al. (2005) found that Landsat 5 TM Band 3 was the best predictor of turbidity in several Minnesota Lakes, and Wang, Han et al. (2006) concluded that Landsat 5 TM Band 2, Band 3/Band 2, Band 4/Band3, and a multivariate regression analysis using Bands 3 and 2 best predicted turbidity in Reelfoot Lake, Tennessee.

The lack of consensus in previous studies is due in part to differences in sediment type, notably particle size and mineral color (Novo, Hansom et al. 1989). Water reflectance is affected by the absorption and scattering properties of sediment. Fine-grained material contains more particles and thus scatters more light than would an equal weight of coarse-grained material (Novo, Hansom et al. 1989). The rock flour in glacial environments is very fine-grained, and thus produces high reflectance/radiance. Since all rock flour is extremely fine-grained, and fine-grained material results in a spectrally more uniform strength of correlation between suspended sediment concentration and reflectance (Novo, Hansom et al. 1989), glacial environments are good candidates for development of a model-based algorithm to measure turbidity from space.

The Bering Glacier, located in coastal, south central Alaska (Figure 1), is the study site for my research. This glacier is the largest (5,174 km^2) and longest (191 km) glacier in continental North America, and it is also the largest temperate surging glacier

on earth (Molnia and Post 1995). The Bering Glacier has surged at least six times during the twentieth century, and the last great surge occurred in 1993-1995 (Molnia and Post 1995). The Glacier is currently retreating, and the observed terminus retreat by year has been mapped using Landsat satellite images (Figure 2).

Recession of the Bering Glacier has resulted in the formation of several ice marginal lakes. The largest of these lakes is Vitus Lake, which is located at the terminus of the Bering Glacier (Figure 1). As the Glacier has retreated, Vitus Lake has expanded rapidly in both area and volume. From 1995 to 2004, Vitus has expanded 95.3 percent in area and 163.1 percent in volume (Josberger, Shuchman et al. 2006). As of 2007, the Lake has an area of 138 km^2 (Shuchman 2007, personal communication). This is a 136.3 percent change in area since 1995. From an evolutionary perspective Vitus Lake is considered highly immature as it was almost non-existent 10 years ago.

Vitus Lake is very cold and deep. Surface temperatures range from near 0 to +2 degrees Celsius, and depths exceed 150 meters in some locations (Josberger, Shuchman et al. 2006). Due to the relative immaturity of the Lake, cold water temperatures, and harsh climate of the region, almost no phytoplankton, zooplankton, or other lower food web organisms exist in Vitus Lake. This was confirmed through a series of plankton and larval fish tows conducted during the 2007 summer field season (Auer 2007, personal communication). Higher food web organisms such as harbor seals, waterfowl, and fish have been observed in Vitus Lake. Interestingly, scat studies of the harbor seals (*Phoca vitulina richardsii*) have revealed only marine prey in their diets, thus indicating only Gulf of Alaska foraging despite their observed residence in Vitus Lake (Savarese 2004).

It is also not known whether the fish reside more permanently in Vitus Lake or if they only seasonally enter the system from the Gulf of Alaska.

The hydrologic routing of the Vitus Lake system is poorly understood due to subglacial and subsurface water movement. Evidence exists, in the form of rock flour in Vitus Lake and moulins on the surface of the glacier, of subglacial and subsurface water movement, but specific locations and amounts of discharge into Vitus Lake are unknown. Known and quantifiable water inputs into Vitus Lake result from glacier melt, overland flow off the surface of the glacier, iceberg calving from the glacier terminus, runoff from the surrounding environment, and discharge from the Tsiviat Lake Basin either through the Abandon River (periodically and currently dry) or other channel. Known water discharge from Vitus Lake occurs primarily through the Seal River which connects Vitus Lake with the Gulf of Alaska.

Management of the Bering Glacier falls under the jurisdiction of the Bureau of Land Management (BLM). The Bering Glacier region is exceptionally diverse and valuable from both an ecological and cultural perspective, and this, in combination with the rapid changes occurring in this environment, makes the Bering Glacier region especially difficult to manage. BLM has provided funding and support over the past decade for research activities to help better understand this unique environment. Each year a remote field camp, managed by the BLM, is populated by researchers from various disciplines and backgrounds.

The goal of my research was to provide the BLM with a remote sensing-based tool to help them better monitor and manage the Bering Glacier region. An ancillary goal was to provide insight into other glacial systems in south central Alaska and the glacial

environments worldwide. My research was focused on the development of an accurate and repeatable method to map turbidity in glacial lakes. Using in situ data and satellite images, I created an algorithm to predict turbidity using multispectral satellite data. Mapped turbidity is useful in discerning sediment dynamics in Vitus Lake and hydrologic routing within the Bering Glacier. Turbidity maps are also useful for detecting change over time and identifying early-warning signs of significant glacial events such as surging or outburst floods.

Methods

In situ turbidity data was collected during the first week of August in 2006 and 2007. Secchi disk data was collected concurrently with the turbidity sampling in 2007. Turbidity data was collected using ALWAS (Automated Lagrangian Water-Quality Assessment System), an autonomous drifter buoy (Figure 3), and secchi disk data was collected using a Wildco 20 cm diameter professional secchi disk (Figure 4).

ALWAS is a free-drifting, sail-powered or electrically propelled, water quality measuring and watershed evaluation buoy. It is capable of measuring a data point with multiple parameters as rapidly as every 40 seconds. Data are transmitted for real-time viewing and are stored for future retrieval and analysis. The stored data are easily downloaded into geographic database (ESRI shapefile) and spreadsheet formats. ALWAS uses advanced sensors to measure water quality parameters and GPS data. ALWAS is the result of a joint partnership between the Michigan Tech Research Institute (MTRI) and the University of Michigan, Marine Hydrodynamics Laboratory.

At the time of data collection, the ALWAS buoy was configured to measure and store onboard, depth, temperature, conductivity, salinity, total dissolved solids, dissolved oxygen, pH, oxidation-reduction potential, turbidity, chlorophyll-a, blue-green algae, nitrates, ammonium, and chlorides. In addition, the ALWAS buoy also provided the full GPS position and navigation suite including not only position but also course and speed over ground.

The sensor head in ALWAS is a YSI 6600 sonde. The turbidity sensor is an optical YSI 6136 Turbidity Probe, and the range of measurement of the sensor is from 0 to 1,000 NTU with a resolution of 0.1 NTU (YSI 2007). The accuracy of the sensor is

plus or minus 2 percent of the reading or 0.3 NTU, whichever is greater (YSI 2007). The performance of the turbidity sensor has been verified through the U.S. Environmental Protection Agency's Environmental Technology Verification Program, and extensive empirical field and laboratory tests document close agreement between in situ measurements made with the sensor and data from a Hach 2100AN – a laboratory instrument recognized as the standard for turbidity measurement (YSI 2007).

ALWAS and secchi disk data was collected at a set of historical sampling stations across Vitus Lake (Figure 5 and Table 2) where CTD (Conductivity Temperature Depth) measurements were recorded for the past seven years. These stations were evenly distributed across the Lake and represented the entire range of sediment distribution found in Vitus. In 2007 data was collected at Sites 1-9 and Sites 14-19. Too many icebergs were present in the western portion of Vitus Lake (Tashalich Arm) to sample at Sites 10-13. In 2006 Sites 1-12 were sampled.

ALWAS data was collected by deploying the buoy upon arrival on station, allowing the buoy to float and collect data while other sampling was occurring, and retrieving the buoy upon station departure. Secchi disk data was collected by lowering the disk at station until no longer visible, raising the disk, and taking a reading at the point when the black and white quadrants became visible. This procedure was repeated until three measurements were recorded for each station, and the mean was calculated for the overall station measurement.

Landsat image scenes were used in this analysis. Landsat is a series of Earth-observing satellites jointly managed by NASA and the USGS. Landsat satellites have been collecting data from space since 1972, and have provided over three decades of

continuous and consistent observations of Earth (NASA). For this reason, Landsat data is very popular with scientists and researchers.

There are currently two Landsat satellites in operation – Landsat 5 TM (Thematic Mapper) and Landsat 7 ETM+ (Enhanced Thematic Mapper Plus). Both Landsat 5 and Landsat 7 are experiencing technical problems. Specifically, Landsat 7 is without its Scan Line Corrector (SLC), which compensates for the forward motion of the satellite. Without the SLC, a series of zigzag patterns (i.e. no data) are visible across the satellite ground track. However, the sensor still acquires 75 percent of the data for any given scene, and the center of the image scene is not affected (NASA).

The ETM+ instrument on the Landsat 7 satellite is an eight-band multispectral scanning radiometer. It detects spectrally-filtered radiation in visible and near infrared (VNIR), shortwave infrared (SWIR), longwave infrared (LWIR), and panchromatic bands. Band 1 detects radiation from 0.45-0.515 µm (blue portion of the electromagnetic (EM) spectrum), Band 2 from 0.525-0.605 µm (blue-green portion of the EM spectrum) , Band 3 from 0.63-0.69 µm (red portion of the EM spectrum), Band 4 from 0.75-0.90 µm (near-infrared (IR) portion of the EM spectrum), Band 5 from 1.55-1.75 µm (mid-IR portion of the EM spectrum), Band 6 from 10.4-12.5 µm (thermal-IR portion of the EM spectrum), Band 7 from 2.09-2.35 µm (mid-IR portion of the EM spectrum), and Band 8 from 0.52-0.9 µm (green to near-IR portion of the EM spectrum) (NASA). EMT+ has a swath width of 183 km, a temporal resolution of 16 days, a spatial resolution of 30 m in Bands 1-5 and Band 7, 60 m in Band 6, and 15 m in Band 8 (NASA). Landsat Bands 1-5 and Band 7 were used in the analysis. Band 6, the thermal band, and Band 8, the panchromatic band, were omitted.

Two Landsat 7 ETM+ images from path 64, row 18 were used in this analysis. The 2006 image was acquired on August 7, 2006, and the 2007 image was acquired on August 10, 2007. Both images were affected by the SLC error, but most of Vitus Lakes fell within the portion of the image scene unaffected. Only a small portion of the Tashlich Arm section of Vitus (far western portion of the Lake) was affected by the SLC error. The images used in this study were acquired from the USGS and were Level 1T (standard terrain correction) products. No additional processing or corrections were applied to the images.

It is important to note that the in situ data and the Landsat satellite data were collected almost concurrently. The 2006 turbidity data was collected August 8th and 9th and the Landsat overpass occurred August 7th. In 2007, the turbidity and secchi disk data was collected August 9th and the Landsat overpass was August 10th.

An average turbidity measurement and an average radiance (this is also the digital number (DN) for the band) for each Landsat 7 band was determined for each station location. At every station, the number of individual turbidity measurements ranged from 6 to 42, and these measurements spanned 1 to 11 pixels. Radiance was determined for each individual turbidity measurement, and these turbidity/radiance measurements were averaged to obtain a single average turbidity and single average radiance for each band at each station. It is important to note that spatial variation of turbidity and average radiance at each site was small (Table 3).

Simple linear regression and multiple linear regression methods were used to create several different model-based algorithms to predict turbidity. The 2007 data was used to create the algorithms, and the algorithms were validated using 2006 data. The

algorithm that produced the best fit was then used to create the turbidity maps of Vitus Lake.

Before the algorithm was applied, the Vitus Lake boundary had to be digitized. The icebergs floating in Vitus Lake and the islands in Vitus Lake also had to be identified and excluded from the area of analysis. Several techniques were used for iceberg and island removal including a slice tool and object-based image classification, but manual identification produced the best results. The automated techniques consistently confused the highly-reflective icebergs with highly-reflective, sediment-laden water in the eastern portion of Vitus Lake, and therefore the automated techniques were not used in this analysis.

The statistical analysis for this project was completed using Minitab 15 statistical software and Microsoft Office Excel 2003, and the spatial analysis and turbidity map generation was completed using ESRI's ArcGIS 9, ArcMap version 9.2 software. The Landsat stacked images were created using ERDAS IMAGINE 9.1 software, and the Landsat gap-filled image products (used only for display in the Figures) was also created using ERDAS.

The turbidity maps of Vitus Lake were created using the Raster Calculator in ArcGIS (included in the Spatial Analyst extension of ArcGIS). Before employing the Raster Calculator, the analysis mask was set to the grid of Vitus Lake with the icebergs and islands removed.

Results

Average turbidity at each site ranged from 3.3-663.9 NTU in 2007 and from 2.2-997.0 NTU in 2006 (Table 3). Average secchi disk depths ranged from 0-13.8 ft in 2007. Average radiance ranged from 51-75 W/(m2*sr*µm) in 2006 and 47-75 W/(m2*sr*µm) in 2007 for Band 1, 33-57 W/(m2*sr*µm) in 2006 and 34-58 W/(m2*sr*µm) in 2007 for Band 2, 20-56 W/(m2*sr*µm) in 2006 and 18-52 W/(m2*sr*µm) in 2007 for Band 3, 10-33 W/(m2*sr*µm) for 2006 and 10-30 W/(m2*sr*µm) in 2007 for Band 4, 10-12 W/(m2*sr*µm) in 2006 and 9-11 W/(m2*sr*µm) in 2007 for Band 5, and 9-11 W/(m2*sr*µm) in 2006 and 8-11 W/(m2*sr*µm) in 2007 for Band 7.

ALWAS turbidity values were log (base 10) transformed (Figure 6 and Figure 7) and their correlation with radiance evaluated (Table 4). In 2007 the highest correlation was between log average turbidity and Band 3 (0.949), and in 2006 the highest correlation was between log average turbidity and Band 4 (0.950). Band 2 also showed relatively high correlations (0.808 for 2007 and 0.882 for 2006) with log average turbidity, but Bands 1, 5, and 7 showed very little if any correlation.

A relatively high correlation (-0.871) was observed between the log secchi data and the log turbidity data (Figure 8). Despite the high correlation between these two variables, only the turbidity data was used in this analysis. Secchi disk measurements were deemed to be inherently a more subjective and thus more prone to inconsistencies and reduced accuracy. The high correlation observed between these variables did indicate the potential use of secchi disk data in the absence of future turbidity data.

Regression Modeling

Bands 3 and 4 were chosen as the independent variables for simple linear regression (SLR) analysis models. The resultant model created from Band 3 radiance and 2007 ALWAS log average turbidity was: Y=-0.329+0.0513*B3. The resultant model created from Band 4 data was: Y=-0.217+0.115*B4. The models fit well with an R^2 of 0.900 and an adjusted R^2 of 0.892 for the Band 3 model, and an R^2 of 0.816 and an adjusted R^2 of 0.802 for the Band 4 model. SLRs using other Landsat bands (Bands 1, 2, 5, and 7) produced R^2 values less than 0.700 and therefore were not used.

Average radiance values from Bands 3 and 4 were both used as independent variables in a multiple linear regression (MLR) analysis. The resultant model was: Y=-0.441+0.0340*B3+0.0507*B4. The MLR model produced an excellent fit with an R^2 value of 0.956 and an adjusted R^2 of 0.949. Other band combinations were used as inputs into MLR models, and while I was able to achieve higher R^2 values, I was unable to achieve a higher adjusted R^2 value than with the combined Band 3 and Band 4 input. Additionally, a MLR model using all of the Landsat bands resulted in p-values statically insignificant for Bands 1, 2, 5, and 7. Thus these bands didn't make a significant contribution to estimating log average turbidity and were not included in the final model.

Model Validation

The 2006 turbidity and Landsat data was not used to create the models. This data was intentionally set aside for validation after the models were created. I used the MLR model and the 2006 Landsat Band 3 and 4 data to determine how well the model predicted the known 2006 turbidity values (Figure 12). Residual and standardized

residual plots (Figure 13) for the model validation analysis showed that all the residuals fall within plus 0.2 and minus 0.3 log NTU from the actual values. Standardized residuals were within plus or minus 1.5 standard deviations from the mean. These small deviations between actual and predicted values indicated the model fit the 2006 data very well.

Turbidity Maps

The MLR model-based algorithm was used to predict log turbidity values at every pixel in Vitus Lake from the 2006 and 2007 Landsat images. The resultant turbidity maps (Figure 14 and Figure 15) showed definite turbidity gradients and turbidity hotspots across Vitus Lake. In general, the maps indicated more sediment loading in 2006.

The 2006 turbidity map showed approximately four locations of high turbidity concentrations in Vitus. These locations were in the far northeastern portion of the Lake, the far southeastern portion of the Lake, along the glacier terminus in the northern portion of the Lake, and in the far southwestern portion of the Lake. The 2007 map showed approximately two locations of high turbidity, and while these locations also displayed high values in 2006, the spatial extents of these turbidity plumes decreased. The high turbidity concentrations from 2007 were located in the far northeastern portion of the Lake and along the glacier terminus in the northern portion of the Lake. The 2007 turbidity map did not contain the far western portion of Vitus Lake (the Tashalich Arm section) because in 2007 too many ice bergs were present to run the algorithm in this area of the Lake.

Discussion and Conclusions

The results of this study are the turbidity maps of Vitus Lake and the model-based algorithm used to create the maps. In the future, this algorithm can be used both forward in backward in time, taking advantage of the long Landsat record available, without the need for further in situ data inputs. All that is required for the algorithm is a Landsat image scene for the area of interest. The algorithm is specifically for use in Vitus Lake, but it also has broader applicability to other lakes within the Bering Glacier region, other glacier-influenced lakes in coastal, south central Alaska, and even similar glacier systems worldwide.

All of the Landsat bands were tested for their suitability in a final turbidity algorithm, but Band 3 and Band 4 as independent variables in a multiple linear regression equation produced the best fit. Recall that Band 3 senses energy in the red portion of the electromagnetic spectrum and Band 4 senses energy in the near infrared portion. Previous studies have identified these portions of the electromagnetic spectrum as useful for detection of sediment in aquatic environments, but previous studies also identified other bands and band combinations as useful without much consensus among the different studies. Further confounding consensus is that previous research activities were conducted in various geographical areas with different factors affecting the aquatic system and remotely-sensed, electro-optical signal. Very little evidence exists of aquatic remote sensing applications in northern environments where conditions are typically more spatially homogeneous, less affected by biological influences, and thus more likely to produce more consistent and accurate results.

The pearson correlation coefficients and the adjusted R^2 values from this analysis are much higher than those reported in other studies. These high values were obtained despite any attempt at a window of analysis or atmospheric correction of the Landsat data. In my search of the literature, I found that most if not all of the other studies involving aquatic remote sensing applications utilize some sort of atmospheric correction, window of analysis, or both to achieve a higher correlation between remote sensing data and ground reference data. Baben (1993) tested windows of 1 by 1, 2 by 2, and 3 by 3 in his research, and found that the 3 by 3 window was the most representative in correlation with his ground reference data. Wang, Han et al. (2006) conducted elaborate atmospheric correction consisting of both radiometric correction and the application of an improved image-based COST (cosign of the solar zenith angle) model before correlating reflectance data and water quality parameters.

In my research, I found that I didn't need to conduct pre-processing of my image scene or utilize a window of analysis for two main reasons. First, as discussed above, my study site was located in a northern environment. Second, the spatially-extensive ALWAS data provided a high-accuracy input data for creation of the algorithm.

The ALWAS data had many different benefits in my research. First, the ALWAS data collected GPS information for each data point. This meant that I was able to accurately assign my turbidity data points to specific Landsat pixels and thus eliminate any errors associated wrong or slightly incorrect GPS information. Second, the ALWAS buoy, as it drifted, provided many data points for each site. With many data points, I was able to take the average and get a more accurate measurement of ground truth. Third, the ALWAS buoy typically covered more than one Landsat pixel. By having several data

points in one pixel and/or data scattered among several pixels, I reduced the potential of problems associated with mixed pixel or edge contamination. In the literature, most studies relied upon single point measurements of ground reference data. This type of research design did not take into account the possibility of the point measurement occurring on the pixel edge nor did it provide enough data to obtain an accurate representation of ground truth.

My turbidity algorithm produced an adjusted R^2 of 0.949, which indicated that the algorithm fit the data very well. Site 17 was the only statistically identified outlier, and this outlier was present in all three of the regression analyses. This site had the highest observed turbidity in 2007 with an average turbidity of 663.9 NTU, and turbidity measurements at this site were much higher than any of the other sites. The next highest average turbidity was 130.5 NTU which was observed at Site 18. Statistically, it might have made sense to remove this outlier, but from a prediction sense, it was important to include this point in the analysis because it represented the upper bound of turbidity values found in Vitus Lake. For this reason, I did not remove this point and decided rather to conduct a log transform of the turbidity data.

The identification of Site 17 as an outlier leads to the conclusion that the algorithm has better prediction power at lower turbidity values. The algorithm could most likely be improved through the inclusion of more points with higher turbidities, but the first step would be to test the prediction power of the current algorithm using more known, high-value turbidity points. The algorithm might also be improved by looking into non-linear fitting techniques or spline fitting.

The turbidity maps of Vitus Lake provide unique insight into sediment dynamics at the Bering Glacier. Mapping of the sediment distribution in Vitus Lake is important because it provides information about the hydrologic routing of the Bering Glacier system. Rock flour is transported to the ice marginal lakes through the glaciers internal plumbing system, and at this point in time, the plumbing is largely unknown. Moulins, which are narrow, tubular chutes or crevasses through which water enters a glacier from the surface (Figure 16), carry freshwater deep into the bowels of the Bering system, but no further evidence of the course or final point of discharge exists. Currently, the best indication of where subglacial discharge occurs is the sediment concentrations in Vitus Lake and the other surrounding ice marginal lakes.

The 2006 and 2007 turbidity maps show several areas of high suspended sediment concentration. These hotspots are most likely where the glacier is discharging sediment-laden freshwater through subsurface conduits. Interestingly, the 2006 map shows more sediment and more sediment hotspots than the 2007 map. This indicates that the hydrologic routing of the Glacier changed between the acquisitions of these two images.

A significant glacial event occurred in late August 2006 that explains many of the inter-annual changes observed in the turbidity maps. While out in the field in early August 2006, we noticed an upwelling of high turbidity, super-cooled water at the terminus of the Glacier in the far northeastern portion of Vitus Lake. It was reported by Jay Fleisher and his team that a gradual, yet progressive leakage occurred at this "plug" location starting in late June 2006, and the failure of this "plug" eventually occurred before the end of the summer melt season (Fleisher, Bailey et al. 2007). Failure of the "plug" resulted from pressure behind the ice dam separating the higher-elevation Tsiviat

Lake Basin from the lower-elevation Vitus Lake. Before failure event, the Tsiviat Lake Basin drained through the Abandon River, but during our August 2007 field work we noticed that the Abandon Channel had dried up and is currently abandoned. This was also confirmed with the 2007 Landsat image (Figure 17).

The turbidity maps showed evidence of the "plug" failure event. First, the Abandon River discharge location in the far southeast portion of the Lake was one of the turbidity hotspots in the 2006 map. The 2007 map did not show any turbidity at the Abandon River discharge location, and thus provided evidence for a change in the hydrologic routing of the system after the failure event. Second, the hotspot locations in the far northeast portion of the Lake and the northern portion of the Lake changed in both sediment concentration and spatial extent between the two years. This was also indicative of a significant change in the hydrologic routing of the system. It appeared as if sediment was being vigorously discharged around the time of the "plug" failure, but one year after the failure, the discharge had lessened. This could have been due to a reduction in pressure associated with the outburst.

It is important to monitor changes in the sediment distribution in Vitus Lake, because changes can be both a precursor and a successor of significant glacier events. As described above, vigorous sediment discharges are associated with "plug" failure events. Similar conditions might occur before a glacier surge event or an outburst flood event. More observations like those reported here will be needed to help identify and differentiate early-warning signals of significant glacial processes.

The user of these turbidity maps and the turbidity algorithm must be cautioned about a few potential problems. The first is that some pixels at the edge of the lake

boundary may show elevated turbidity values. This could be a result of bottom
reflectance occurring in areas of shallow, clear water, or could be the result of shoreline
contamination where the pixel may not actually contain lake area (due to poor
digitization of the lake boundary) or the pixel may contain a mixture of land and lake area
(due to the spatial resolution of the satellite sensor). With any of the above scenarios the
pixel is not reflecting an actual turbidity measurement and should be ignored. Another
potential problem, similar to the first, is the possibility of bottom reflectance in shallow
areas of the Lake. Vitus Lake is extremely deep in most areas, but this could be a concern
in the far southwest portion of the Lake. The 2006 turbidity map (Figure 14) shows a
turbidity hot spot in this section of the Lake, and it is difficult to determine if this is the
result of subglacial discharge or shallow water. From the Vitus Lake bathymetry data
(Josberger, Shuchman et al. 2006), we know that this portion of the lake is shallower, but
it is difficult to know whether bottom reflectance is occurring. My experience indicates
that bottom reflectance is not occurring, and the turbidity hotspot in this location is due to
glacial discharge.

Future Research

The next step for further research in this field would be to apply the turbidity
algorithm to other lakes in the Bering Glacier region. From satellite images I have
observed definite differences in turbidity among the lakes, and interestingly, I have
observed stark turbidity differences among lakes in close proximity to one another
despite any obvious surface connections (Figure 18). Information obtained from the
running the turbidity algorithm on these lakes may provide insight into the hydrologic
routing of the Glacier. At this point it appears as if the Glacier is discharging sediment-

laden water into some of the lakes through underground conduits. If this is the case, some of these conduits would have to cover relatively large distances and have highly localized discharge locations.

Future research activities could be focused on further inter- and intra-annual comparisons of turbidity maps. By running the algorithm on several Landsat images throughout a single year, we would be able to gain insight into the seasonal dynamics of sediment distribution. Through yearly comparisons of turbidity maps created using historical Landsat data, we would be able to quantify and better understand how the sediment distribution changes over a larger time period. We could also look into how sediment loading is affected by glacier surge and retreat.

Both Landsat 5 and 7 are experiencing technical difficulties, and both satellites have performed beyond their expected life span. The Landsat Data Continuity Mission (LDCM) is currently seeking replacement options for the old and ailing Landsat satellites in orbit, but the next-generation Landsat satellite is not expected to be launched until 2011 (USGS). Despite the uncertainties surrounding the Landsat program, other platforms exist that could provide an input data replacement for the algorithm. For example, ASTER (Advanced Spaceborne Thermal Emission and Reflection Radiometer) is a viable alternative. ASTER is an instrument on the Terra EOS (Earth Observing System) satellite launched December 1999 (JPL). ASTER captures data in 14 bands ranging from the visible to the thermal infrared wavelengths. ASTER Bands 2 and 3 (0.63-0.69 µm and 0.76-0.86 µm, respectively) are almost exactly the same as Landsat EMT+ Bands 3 and 4 (Table 1). The spatial resolution of ASTER Bands 2 and 3 (15 m) are also similar to Landsat EMT+ Bands 3 and 4 (30 m) (JPL).

The algorithm developed as part of this research is applicable to other glaciers in coastal, south central Alaska. Along the coast there are many other glacial systems similar to the Bering Glacier, and my algorithm could be useful in determining glacier dynamics and sediment loading from a regional perspective. This algorithm is also applicable to all lake systems affected by sediment-laden glacial discharge.

The algorithm may have to be slightly tweaked (i.e. the coefficients adjusted) in order to be more broadly applicable to regional and global systems, and this would be accomplished through the inclusion of more data points. Ideally, ALWAS turbidity data points would be best, but in the situations where this type of data isn't available, turbidity data collected using traditional sampling techniques or secchi disk data could be substituted. Recall from the results section of this paper that a strong correlation was observed between the turbidity and secchi disk data. Secchi disk data wouldn't be ideal, but it does offer a low-cost alternative. Additionally, since the secchi disk has been available since 1865 (Cole 1994), historical secchi data may be obtainable in some locations. Historical data would provide important data points from the perspective of a time series analysis.

In the face of a changing climate and political uncertainty it is more important than ever to monitor glaciers and their associated environments. Glacial environments will be the first affected by a warmer climate, and these environments have the potential to act as early-warning systems, but we need more data to support scientific claims. My algorithm has the potential to provide data, and provide this data remotely and at reduced cost over traditional, field-based data collection efforts.
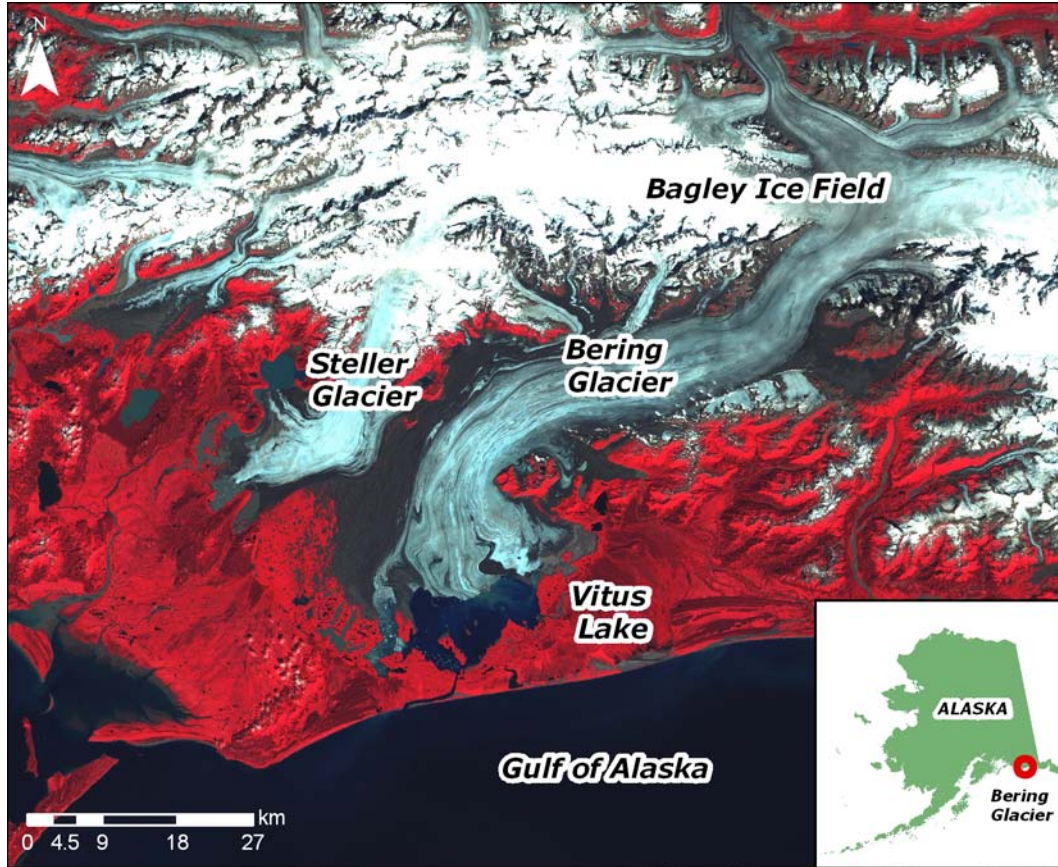
Image Source: Landsat 7 August 10, 2007

Figure 1. The Bering Glacier is located in coastal, south central Alaska. Vitus Lake, a large ice marginal lake, resides at the terminus of the Bering Glacier.
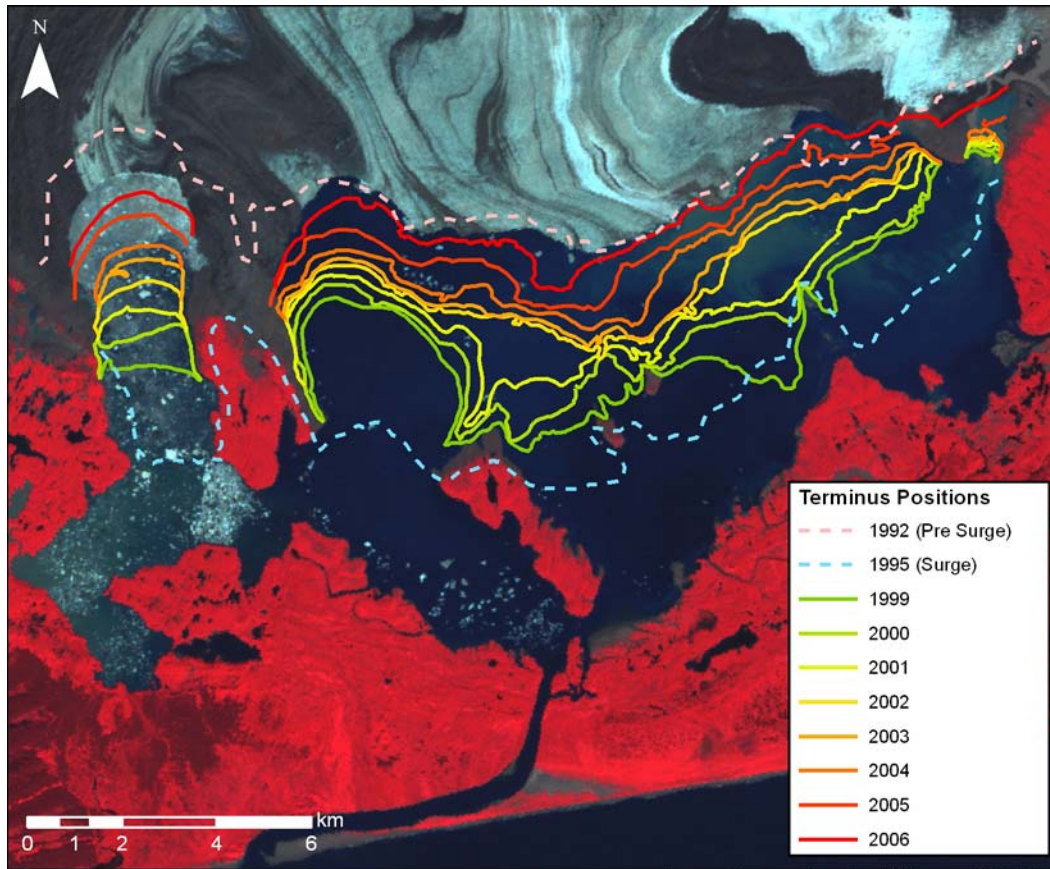
Figure 2. The Bering Glacier is the largest temperate surging glacier on earth. Bering is currently retreating, and terminus retreat since the most recent 1993-1995 surge mapped using Landsat satellite images is shown above.

Figure 3. ALWAS is an autonomous drifter buoy that measures various water quality parameters, including turbidity, as a function of location. ALWAS was deployed in Vitus Lake during the 2006 and 2007 summer field seasons.

Figure 4. Secchi disk depth measurements were taken in Vitus Lake during the 2007 summer field season. A Wildco 20 cm professional secchi disk was used for sampling.
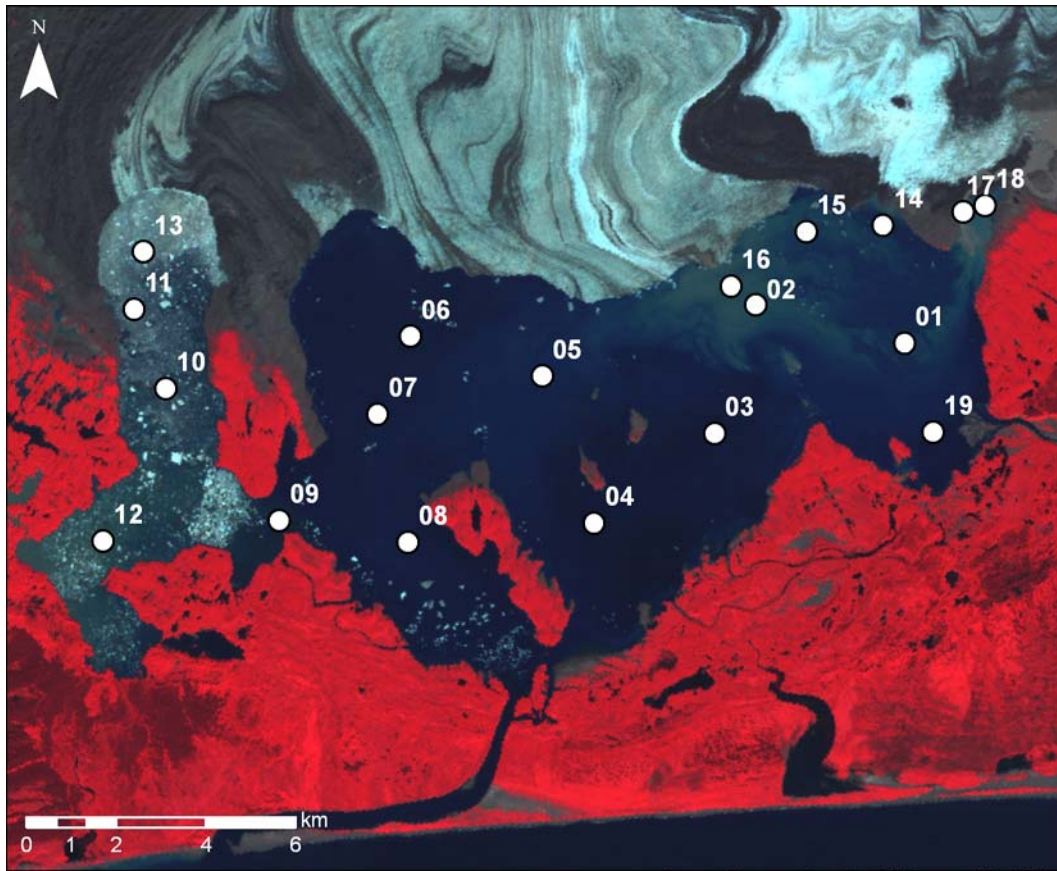
Image Source: Landsat 7 August 10, 2007

Figure 5. Turbidity and secchi disk data was collected at a set of historical sampling site locations across Vitus Lake. These sites are evenly distributed and represent the entire range of turbidity values found in Vitus Lake.
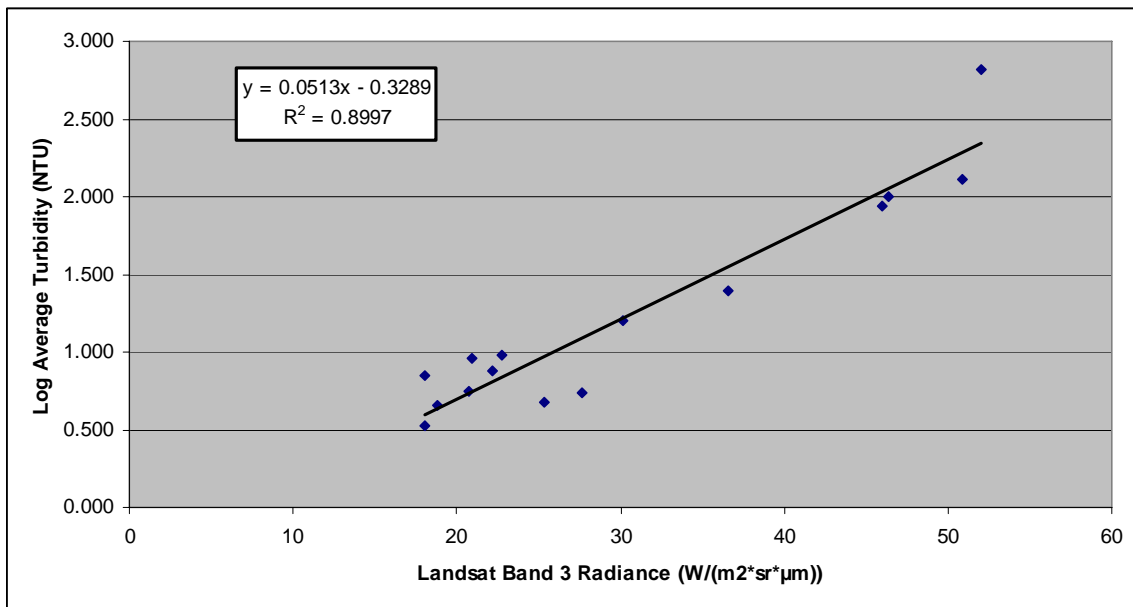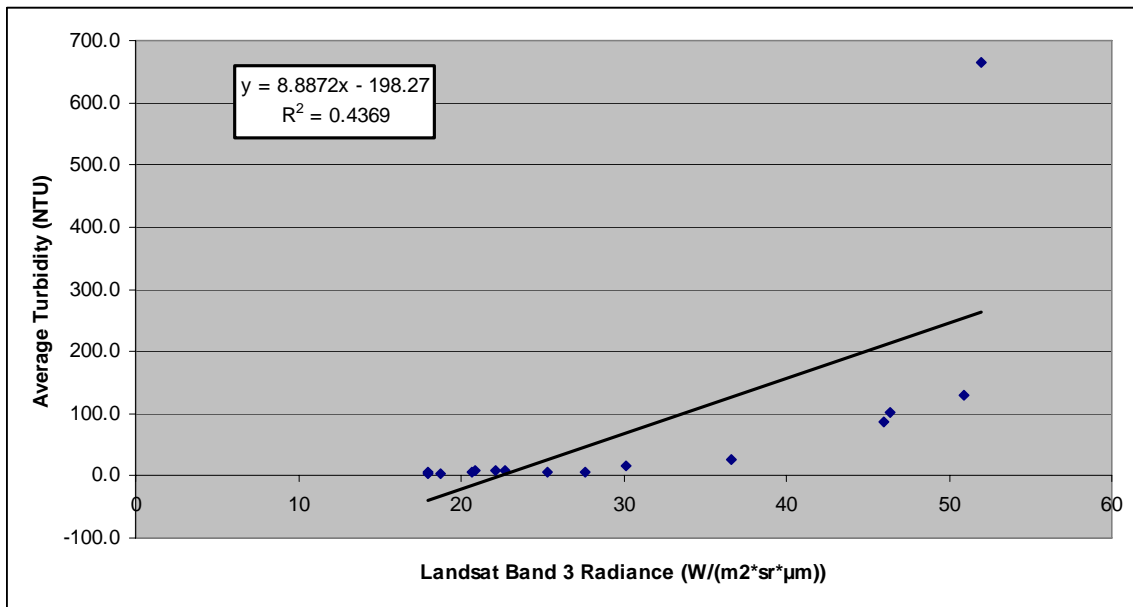
Figure 6. Scatterplots for Landsat Band 3 radiance versus average turbidity (top) and log average turbidity (bottom) provide evidence for a log transform of the turbidity data. The top plot shows a non-linear relationship between radiance and average turbidity, while the bottom plot shows a linear relationship. Note the data transformation increased the R^2 from 0.4369 to 0.8997.

30
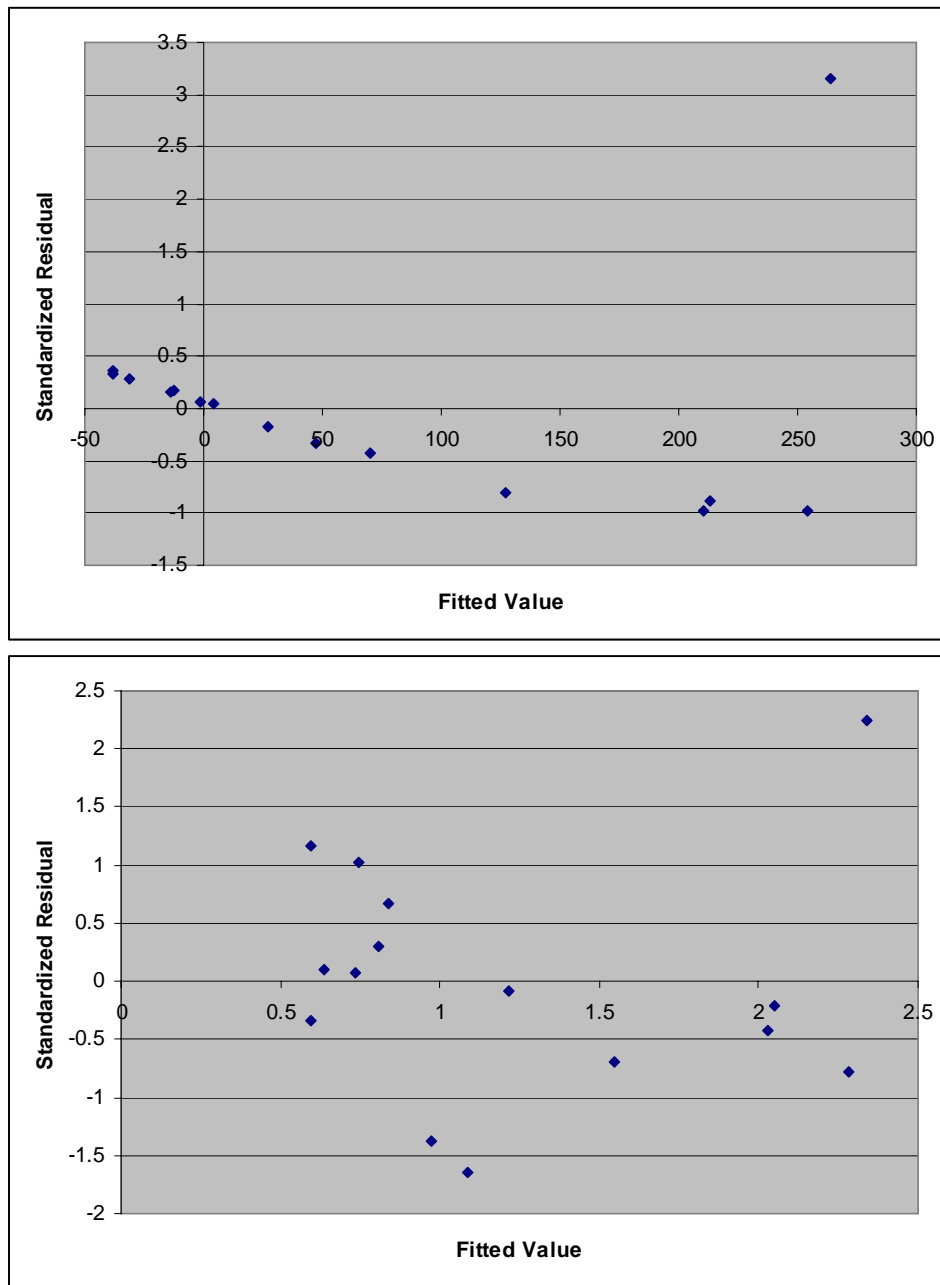
Figure 7. Residual plots showing the fit of a straight line to the log average turbidity (bottom) and non-log data (top) using Landsat Band 3 as the predictor variable are further evidence for a log transform of the turbidity data. The residuals in the log plot (bottom) are mostly centered around zero with points both above and below the zero line. In the non-log plot (top) residuals display a definite pattern and do not appear to occur at random. The log transformation also brings the outlier in the upper right corner of the non-log plot into slightly more than two standard deviations from the mean from slightly more than three.
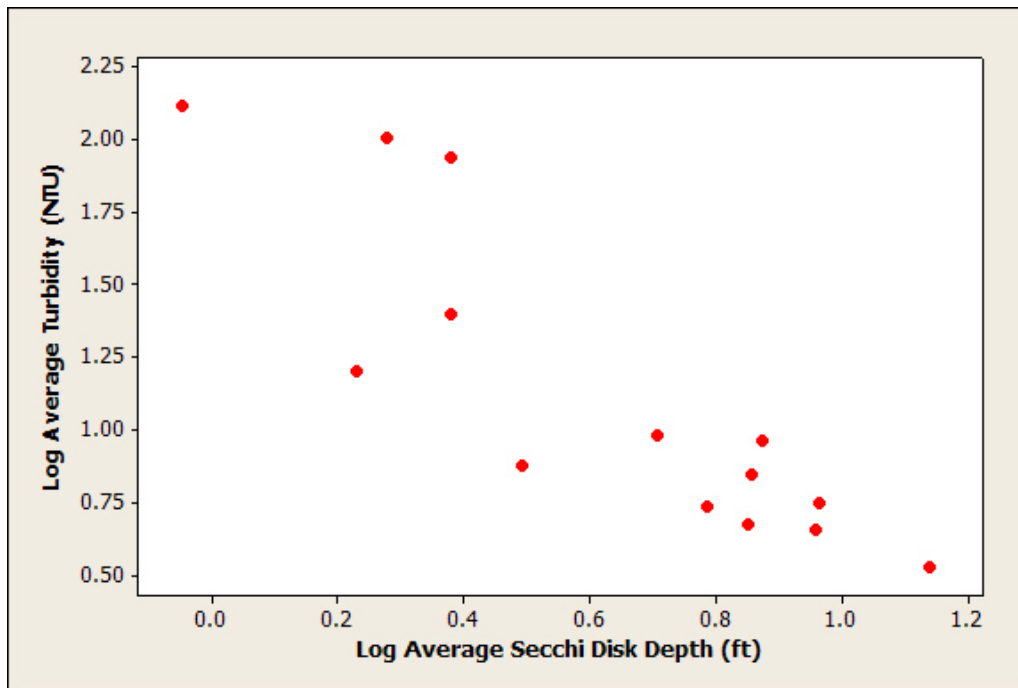
Figure 8. A scatterplot of log average secchi disk depth versus log average turbidity shows a relatively strong negative correlation between the two variables. A pearson correlation coefficient of -0.871 was observed for these two variables.

```
The regression equation is
Log Av Turb = - 0.329 + 0.0513 Band 3_1


Predictor        Coef    SE Coef       T        P
Constant      -0.3289     0.1557   -2.11    0.055
Band 3_1     0.051344   0.004754   10.80    0.000


S = 0.223351    R-Sq = 90.0%    R-Sq(adj) = 89.2%


Analysis of Variance


Source            DF       SS       MS         F       P
Regression         1   5.8193   5.8193   116.65    0.000
Residual Error    13   0.6485   0.0499
Total             14   6.4678


Unusual Observations
              Log Av
Obs  Band 3_1    Turb     Fit   SE Fit   Residual   St Resid
 13      52.0  2.8221  2.3410   0.1177     0.4811      2.53R


R denotes an observation with a large standardized residual.
```


Figure 9. Statistical output and standardized residual plots for the SLR model created using Band 3 as the predictor variable.

```
The regression equation is
Log Av Turb = - 0.217 + 0.115 Band 4_1


Predictor      Coef   SE Coef      T      P
Constant    -0.2165    0.2060   -1.05   0.312
Band 4_1    0.11494   0.01512    7.60   0.000


S = 0.302263   R-Sq = 81.6%   R-Sq(adj) = 80.2%


Analysis of Variance

Source          DF      SS      MS      F      P
Regression       1   5.2801  5.2801  57.79  0.000
Residual Error  13   1.1877  0.0914
Total           14   6.4678


Unusual Observations
             Log Av
Obs  Band 4_1   Turb     Fit  SE Fit  Residual  St Resid
 13      29.5  2.8221  3.1742  0.2671   -0.3521    -2.49RX


R denotes an observation with a large standardized residual.
X denotes an observation whose X value gives it large leverage.
```
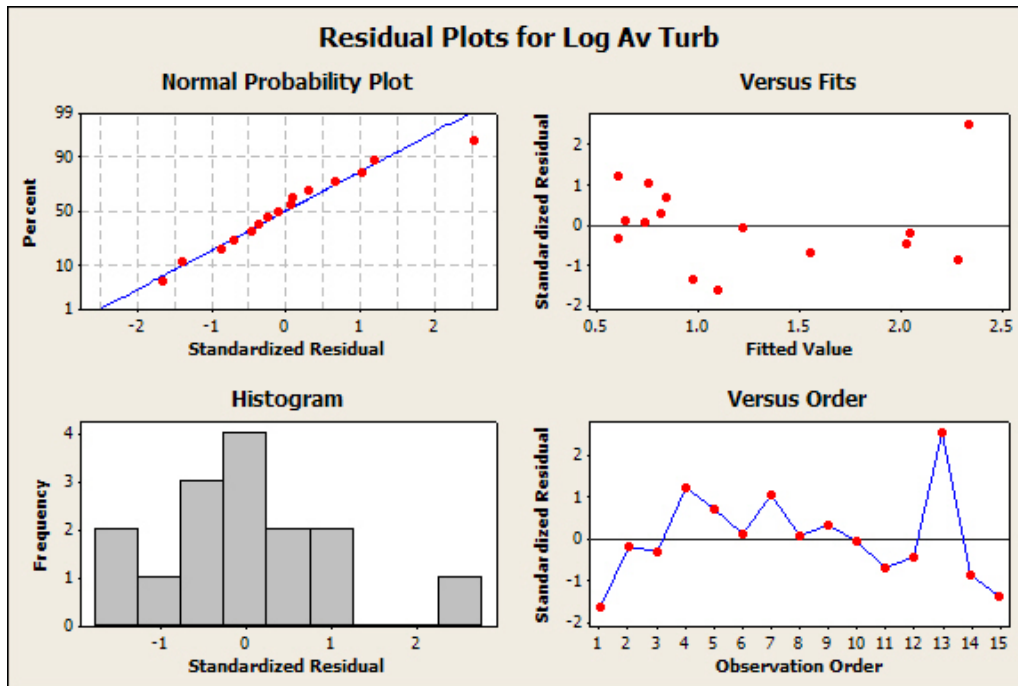

Figure 10. Statistical output and standardized residual plots for the SLR model created using Band 4 as the predictor variable.

34

```
The regression equation is
Log Av Turb = - 0.441 + 0.0340 Band 3_1 + 0.0507 Band 4_1

Predictor       Coef    SE Coef       T        P
Constant     -0.4407     0.1111    -3.97    0.002
Band 3_1    0.034000   0.005515     6.17    0.000
Band 4_1     0.05071     0.01296     3.91    0.002

S = 0.154105    R-Sq = 95.6%    R-Sq(adj) = 94.9%

Analysis of Variance

Source             DF       SS       MS        F       P
Regression          2   6.1828   3.0914   130.17   0.000
Residual Error     12   0.2850   0.0237
Total              14   6.4678

Source      DF   Seq SS
Band 3_1     1   5.8193
Band 4_1     1   0.3635

Unusual Observations
              Log Av
Obs   Band 3_1   Turb      Fit   SE Fit   Residual   St Resid
 13       52.0  2.8221   2.8231   0.1476    -0.0010      -0.02 X

X denotes an observation whose X value gives it large leverage.
```
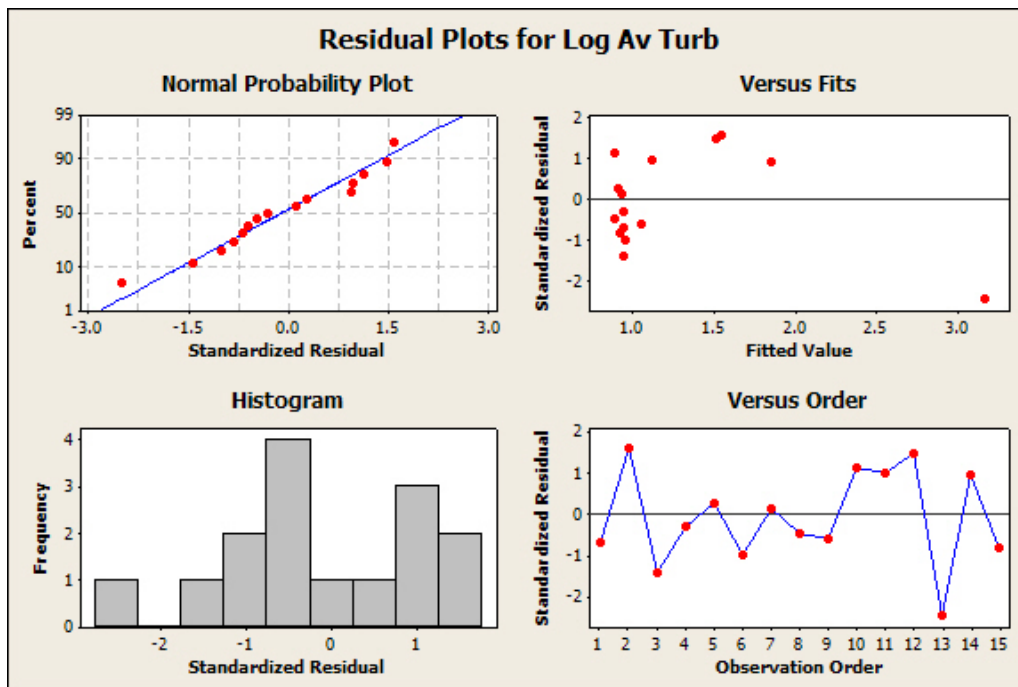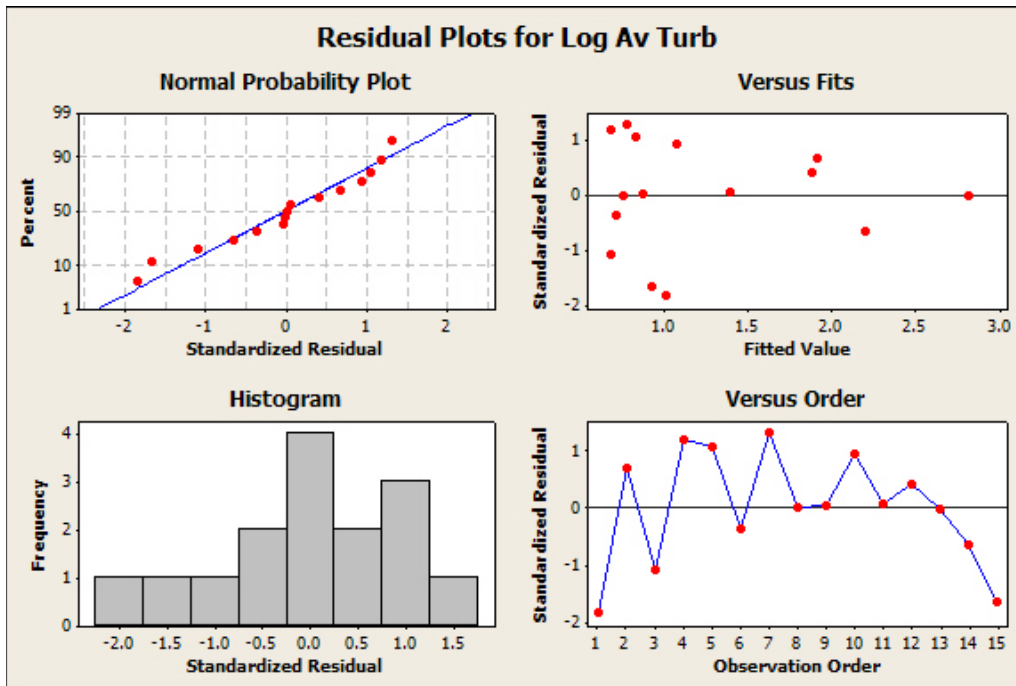

Figure 11. Statistical output and standardized residual plots for the MLR model created using Band 3 and Band 4 as the predictor variables.

35
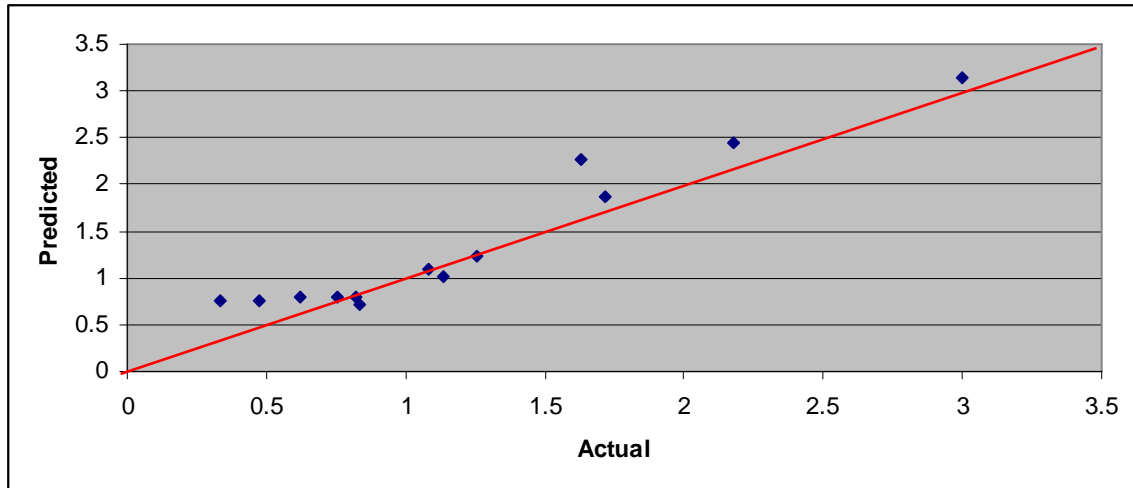
Figure 12. A model validation test was conducted using 2006 turbidity data. A scatterplot of the actual log turbidity values verses the predicted values derived from the MLR model shows relatively good fit. The red line indicates the line of perfect fit, and most of the points fall close to this line.
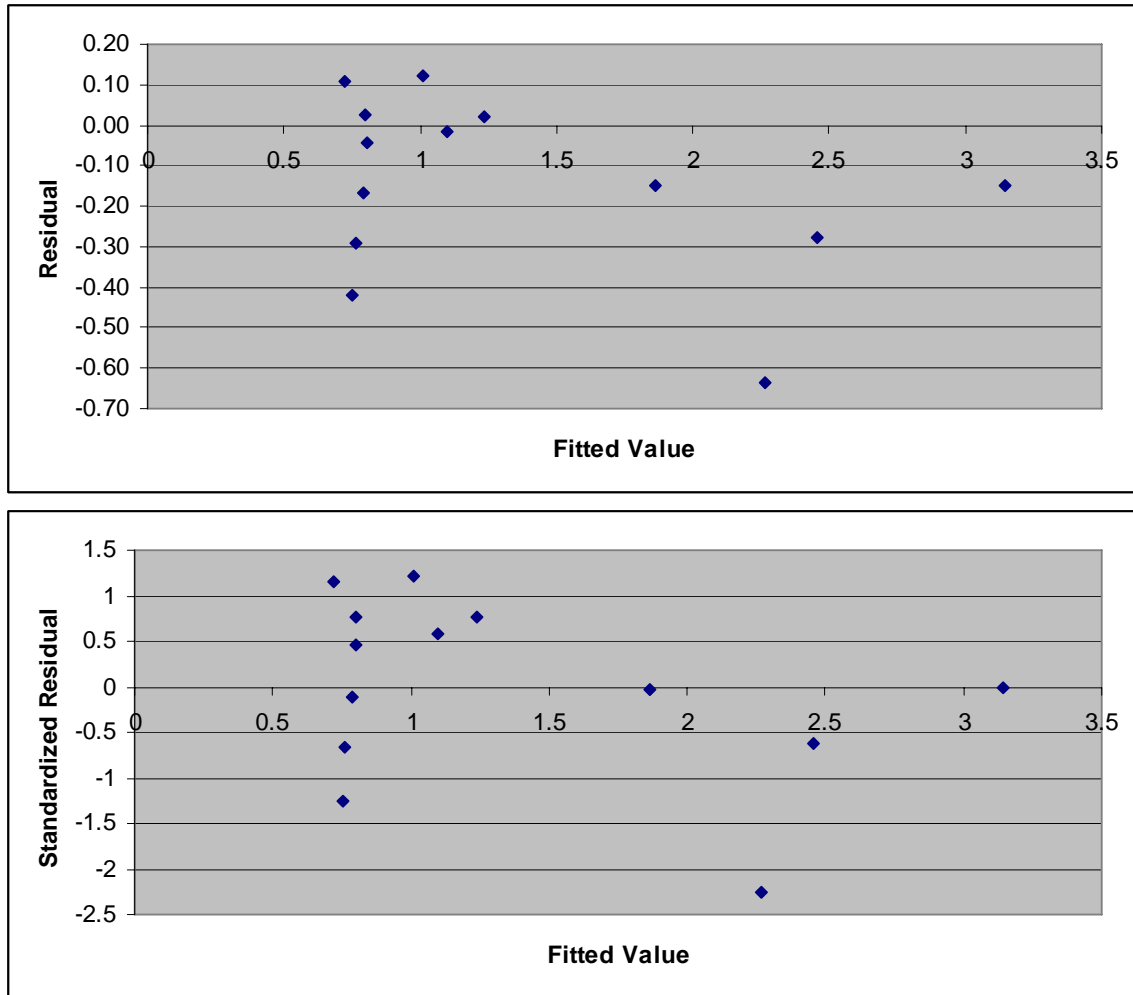
Figure 13. Residual (top) and standardized residual (bottom) plots from the model validation test show that the model fits the data well. Residuals are relative small (top) and standardized residuals are approximately plus or minus 1.5 standard deviations from the mean (bottom).
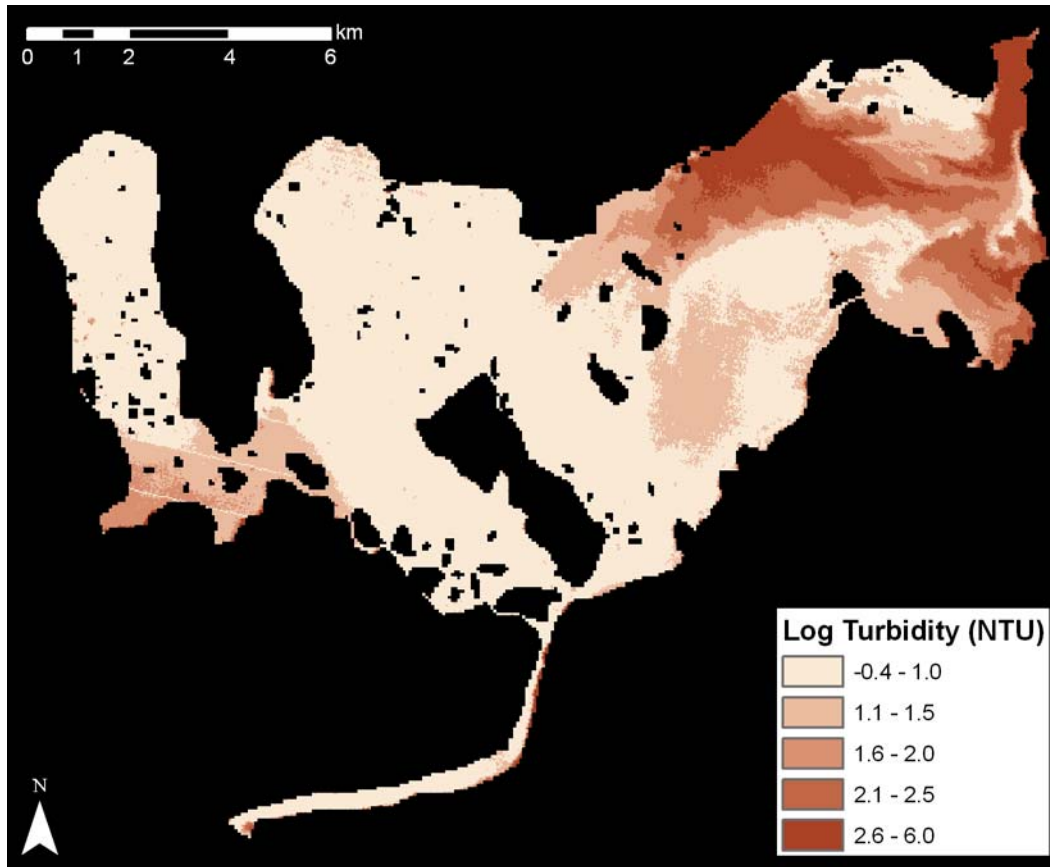
Figure 14. The 2006 Vitus Lake turbidity map shows approximately four turbidity hotspot in Vitus Lake. These hotspots occur in the far northeastern portion of the Lake, the far southeastern portion of the Lake, along the glacier terminus in the northern portion of the Lake, and in the far southwestern portion of the Lake.
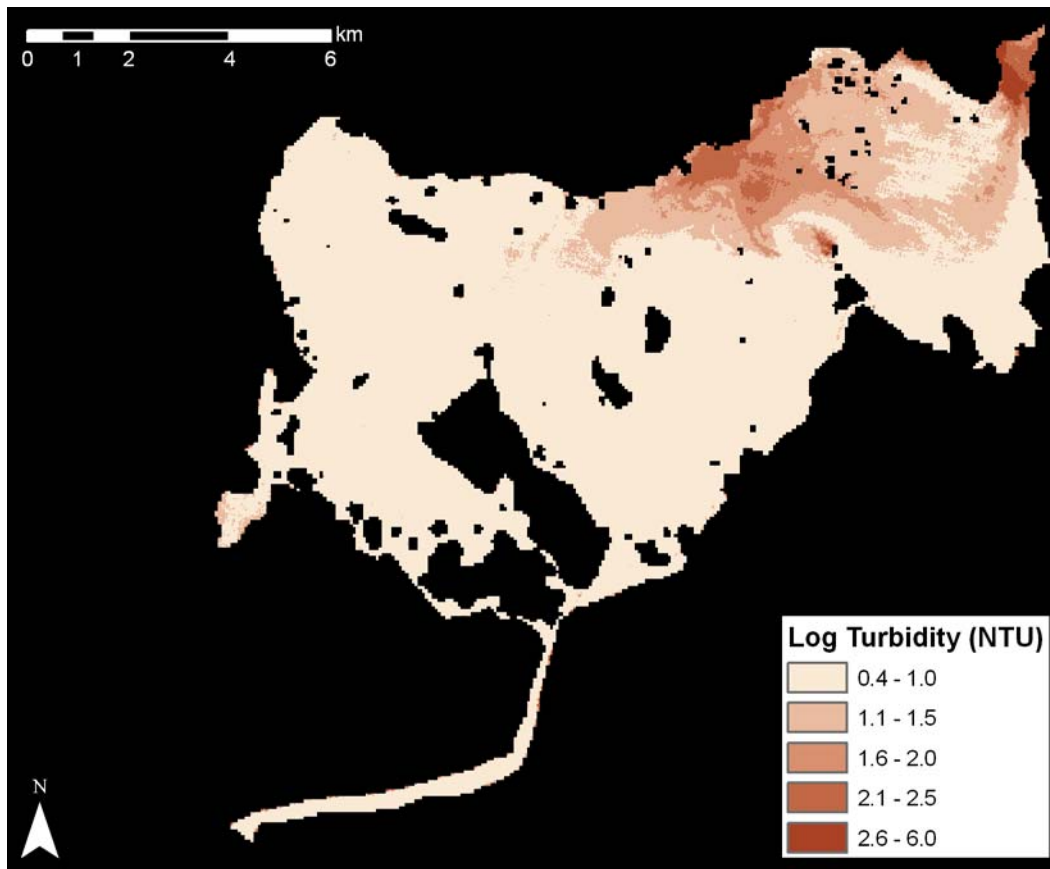
Figure 15. The 2007 Vitus Lake turbidity map shows approximately two turbidity hotspots in Vitus Lake. These hotspots occur in the far northeastern portion of the Lake and along the glacier terminus in the northern portion of the Lake.

Figure 16. Moulins are common features on the Bering Glacier. Moulins are narrow, tubular chutes or crevasses through which water enters a glacier from the surface.

Figure 17. The "plug" failure that occurred before the end of the 2006 melt season resulted in several changes in the landscape and the hydrologic routing of the glacier system. The "plug" is marked with a yellow star in both images. The 2006 image (top) was acquired before the event, and this image shows the conditions prior to the failure event. The event changed the outflow location of the Tsiviat Lake Basin which drained in 2006 through the Abandon River and is currently draining through the "plug" location (bottom image). Note that the Abandon River is no longer discharging sediment into Vitus Lake (bottom image).
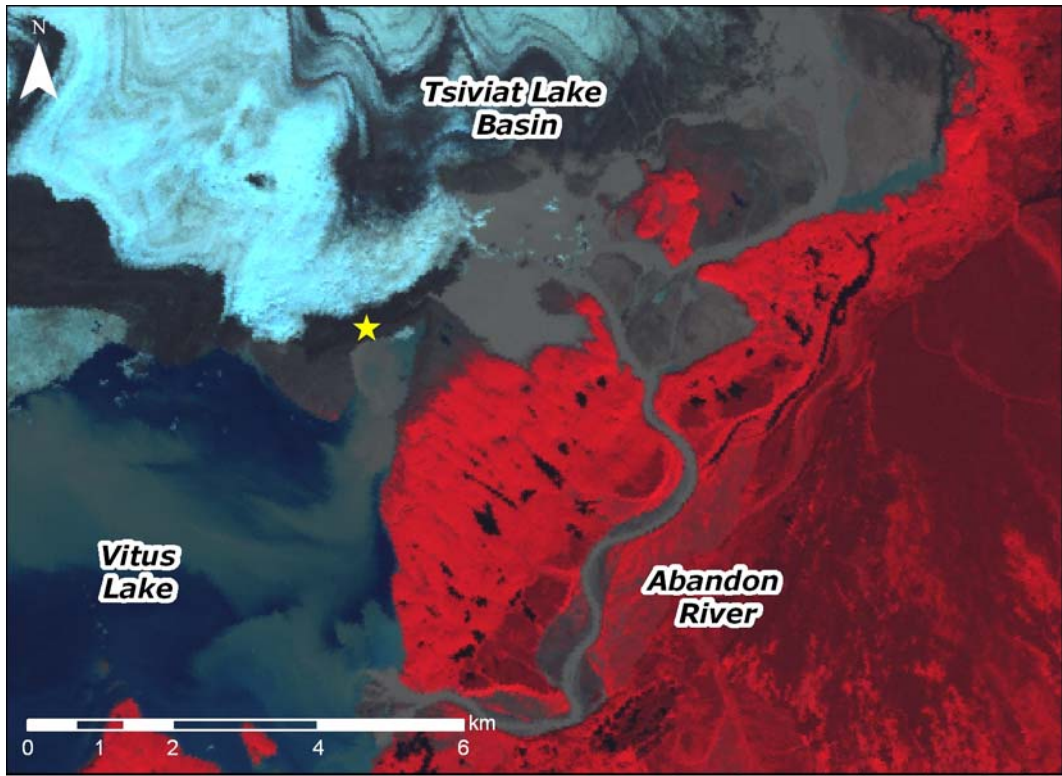
Image Source: Landsat 7 August 7, 2006
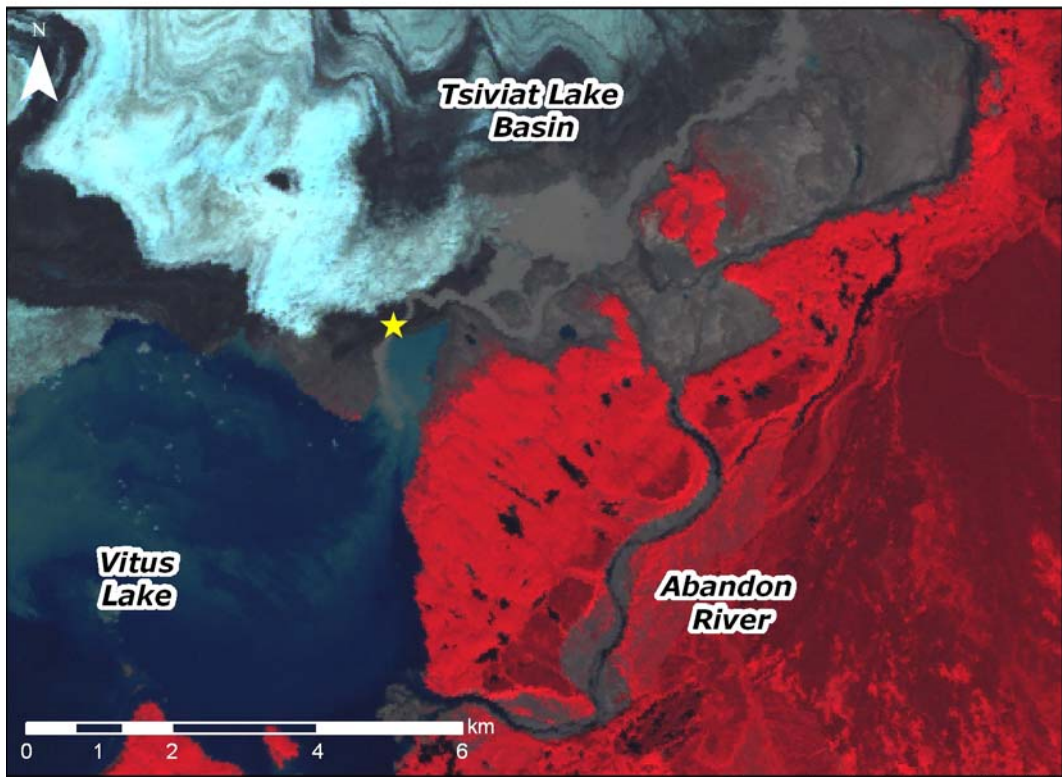
Image Source: Landsat 7 August 10, 2007

Figure 17.
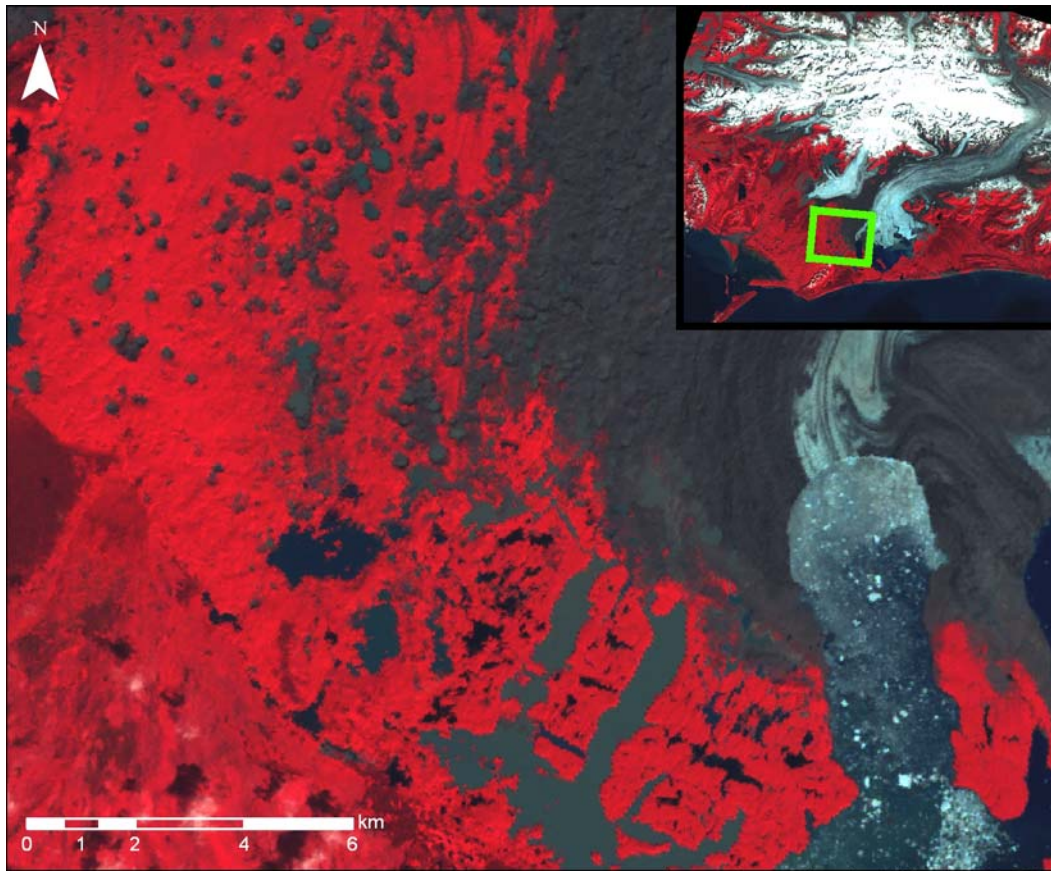
Image Source: Landsat 7 August 10, 2007

Figure 18. Large turbidity differences exist among surrounding lakes in the Bering Glacier region. These lakes have very different turbidity concentrations despite their close geographical proximity. These differences in turbidity could be indicative of subsurface glacier discharge through underground conduits.

Table 1. Landsat 5 and Landsat 7 are the two most recent Landsat satellites. While the sensors on these satellites are similar, there are slight differences in the portions of the electromagnetic spectrum sensed for each band and the total number of bands.

Band Number	Landsat 7 ETM+ (μm)	Landsat 5 TM (μm)	Portion of Electromagnetic Spectrum
Band 1	0.45-0.515	0.45-0.52	Blue
Band 2	0.525-0.605	0.52-0.60	Green
Band 3	0.63-0.69	0.63-0.69	Red
Band 4	0.75-0.90	0.76-0.90	Near-infrared
Band 5	1.55-1.75	1.55-1.75	Mid-infrared
Band 6	10.4-12.5	10.4-12.5	Thermal-infrared
Band 7	2.09-2.35	2.08-2.35	Mid-infrared
Band 8	0.52-0.9	NA	Green to near-infrared

Table 2. Turbidity and secchi disk data was collected at a set of historical sampling sites across Vitus Lake. GPS coordinates for these sites are presented below.

Site Number	Latitude*	Longitude*
01	60.149617	-143.303783
02	60.156233	-143.364333
03	60.130150	-143.378983
04	60.111433	-143.426067
05	60.140400	-143.449133
06	60.147383	-143.502567
07	60.131483	-143.514567
08	60.106200	-143.500533
09	60.109600	-143.552533
10	60.135050	-143.600233
11	60.150717	-143.614150
12	60.104100	-143.623117
13	60.162283	-143.611367
14	60.173140	-143.314130
15	60.171290	-143.344900
16	60.159800	-143.374440
17	60.176310	-143.282100
18	60.177830	-143.273320
19	60.131960	-143.291170

*Datum NAD 83

Table 3. A summary of the values obtained for average radiance (W/(m2*sr*μm)) for Landsat Bands 1-5 and Band 7, average turbidity (NTU), and average secchi disk depth (ft) for each site are presented below.

| Site | 2006 | | | | | | | 2007 | | | | | | | |
	B1	B2	B3	B4	B5	B7	Av. Turb.	B1	B2	B3	B4	B5	B7	Av. Turb.	Av. Secchi
01	68	55	50	20	10	10	42.7	69	48	28	10	9	9	5.4	6.1
02	69	55	52	22	11	10	149.5	68	51	46	15	9	8	101.1	1.9
03	75	50	29	11	10	9	12.0	58	34	18	10	10	9	3.3	13.8
04	66	39	20	10	10	10	6.8	57	34	18	10	10	11	7.0	7.2
05	69	46	26	12	10	10	13.7	72	45	23	10	10	10	9.6	5.1
06	67	40	21	10	10	9	6.7	59	36	19	10	11	8	4.5	9.1
07	66	40	21	10	10	10	5.7	64	40	21	10	10	9	9.2	7.5
08	63	39	21	10	10	10	4.2	62	38	21	10	11	10	5.6	9.2
09	55	42	32	12	10	9	18.1	47	35	22	11	10	9	7.5	3.1
10	51	33	21	10	10	10	3.0	NA	NA	NA	NA	NA	NA	NA	NA
11	52	34	20	10	10	10	2.2	NA	NA	NA	NA	NA	NA	NA	NA
12	58	45	43	17	10	9	51.9	NA	NA	NA	NA	NA	NA	NA	NA
14	NA	NA	NA	NA	NA	NA	NA	68	48	30	10	10	9	15.9	1.7
15	NA	NA	NA	NA	NA	NA	NA	69	52	37	12	9	10	25.0	2.4
16	NA	NA	NA	NA	NA	NA	NA	68	51	46	15	9	8	87.0	2.4
17	NA	NA	NA	NA	NA	NA	NA	72	57	52	30	10	10	663.9	0
18	NA	NA	NA	NA	NA	NA	NA	75	58	51	18	10	11	130.5	0.9
19	NA	NA	NA	NA	NA	NA	NA	68	46	25	10	9	9	4.7	7.1
Plug	71	57	56	33	12	11	997.0	NA	NA	NA	NA	NA	NA	NA	NA

Table 4. Pearson correlation coefficients for log average turbidity and Landsat band average radiance show consistently high correlations for Bands 3 and 4 for the two years.

	2007 Log Average Turbidity	**2006 Log Average Turbidity**
Band 1	0.566	0.479
Band 2	0.808	0.882
Band 3	0.949	0.938
Band 4	0.904	0.950
Band 5	-0.185	0.909
Band 7	0.039	0.482

Acronyms

ALWAS – Automated Lagrangian Water-Quality Assessment System

ASTER – Advanced Spaceborne Thermal Emission and Reflection Radiometer

CPAs – Color Producing Agents

CTD – Conductivity temperature depth

BLM – Bureau of Land Management

DN – Digital Number

EM – Electromagnetic

EOS – Earth Observing System

ETM+ – Enhanced Thematic Mapper Plus

IR – Infrared

LWIR – Longwave infrared

MLR – Multiple Linear Regression

MODIS – Moderate Resolution Imaging Spectroradiometer

MTRI – Michigan Tech Research Institute

NASA – National Aeronautics and Space Administration

NTU – Nephelometric Turbidity Unit

SeaWiFS – Sea-viewing Wide Field-of-view Sensor

SLC – Scan Line Correction

SLR – Simple Linear Regression

SWIR – Shortwave infrared

USGS – United States Geological Survey

VNIR – Visible and near infrared

Literature Cited

Auer, Nancy (2007). Personal Communication.

Baban, Serwan M. J. (1993). "Detecting water quality parameters in the Norfolk Broads, U.K., using Landsat imagery." International Journal of Remote Sensing **14**(7): 1247-1267.

Brezonik, Patrick, Kevin D. Menken and Marvin Bauer (2005). "Landsat-based Remote Sensing of Lake Water Quality Characteristics, Including Chlorophyll and Colored Dissolved Organic Matter (CDOM)." Lake and Reservoir Management **21**(4): 373-382.

Cole, Gerald A. (1994). Textbook of Limnology, Waveland Press, Inc.

Fleisher, P. Jay, Palmer K. Bailey and Eric M. NATEL (2007). Ice Dam Breakout at Bering Glacier, Alaska. Geological Society of America 2006 Annual Meeting. Philadelphia, PA.

Josberger, E.G., R.A. Shuchman, G.A. Meadows, S. Savage and J. Payne (2006). "Hydrography and Circulation of Ice-marginal Lakes at Bering Glacier, Alaska, U.S.A." Arctic, Antarctic and Alpine Research **38**(4): 547-560.

JPL, NASA. "ASTER: Advanced Spaceborne Thermal Emission and Reflection Radiometer." 2007, from http://asterweb.jpl.nasa.gov/index.asp.

Molnia, Bruce F. and Austin Post (1995). "Holocene History of Bering Glacier, Alaska: A Prelude to the 1993-1994 Surge." Physical Geography **16**(2): 87-117.

NASA. "The Landsat Program." from http://landsat.gsfc.nasa.gov/.

Novo, E. M. M., J. D. Hansom and P. J. Curran (1989). "The effect of sediment type on the relationship between reflectance and suspended sediment concentration." International Journal of Remote Sensing **10**(7): 1283-1289.

Pozdnyakov, Dmitry and Hartmut Grassl (2003). Colour of Inland and Coastal Waters: A Methodology for Its Interpretation, Praxis Publishing Ltd.

Pozdnyakov, Dmitry, Robert Shuchman, Anton Korosov and Charles Hatt (2005). "Operational algorithm for the retreival of water quality in the Great Lakes." Remote Sensing of Environment **97**: 352-370.

Savarese, Danielle M. (2004). Seasonal trends in harbor seal (*Phoca vitulina richardsii*) abundance at the Bering Glacier in south central Alaska, University of Alaska Anchorage. **M.S.:** 70.

Shuchman, Robert (2007). Personal Communication.

Shuchman, Robert, Anton Korosov, Charles Hatt, Dmitry Pozdnyakov, Jay Means and Guy Meadows (2006). "Verification and Application of a Bio-optical Algorithm for Lake Michigan Using SeaWiFS: a 7-year Inter-annual Analysis." Journal of Great Lakes Research **32**: 258-279.

Upper Midwest Regional Earth Science Applications Center, (RESAC). "Regional Water Clarity." from http://resac.gis.umn.edu/water/regional_water_clarity/regional_water_clarity.htm.

USGS. "Landsat Data Continuity Mission." 2007, from http://ldcm.usgs.gov/LDCMHome.php.

Wang, F., L. Han, H.-T. Kung and R. B. Van Arsdale (2006). "Applications of Landsat-5 TM imagery in assessing and mapping water quality in Reelfoot Lake, Tennessee." International Journal of Remote Sensing **27**(23): 5269-5283.

YSI. (2007). "YSI 6136 Turbidity Sensor Spec Sheet." from https://www.ysi.com/DocumentServer/DocumentServer?docID=EMS_E56_6136 TURBIDITY.